Localization in underwater dispersive channels using the time-frequency-phase continuity of signals

Cornel Ioana, Arnaud Null Jarrot, Cedric Gervaise, Yann Stephan, André Quinquis

Localization in Underwater Dispersive Channels Using the Time-Frequency-Phase Continuity of Signals

Cornel Ioana, Arnaud Jarrot, Cédric Gervaise, Yann Stéphan, and André Quinquis

***Abstract*—Time-frequency representations constitute the main tool for analysis of nonstationary signals arising in real-life systems. One of the most challenging applications of time-frequency representations deal with the analysis of the underwater acoustic signals. Recently, the interest for dispersive channels increased mainly due to the presence of the wide band nonlinear effect at very low frequencies. That is, if we intend to establish an underwater communication link at low frequencies, the dispersion phenomenon has to be taken into account. In such conditions, the application of the conventional time-frequency tools could be a difficult task, mainly because of the nonlinearity and the closeness of the time-frequency components of the impulse response. Moreover, the channel being unknown, any assumption about the instantaneous frequency laws characterizing the channel could not be approximate. In this paper, we introduce a new time-frequency analysis tool that aims to extract the time-frequency components of the channel impulse response. The main feature of this technique is the joint use of time-amplitude, time-frequency, and time-phase information. Tests provided for realistic scenarios and real data illustrate the potential and the benefits of the proposed approach.**

***Index Terms*—Dispersive channels, time-frequency analysis, time-varying systems, underwater acoustics.**

I. Introduction

THE field of signal analysis is a very important element in a system of representation and/or information extraction. Considering the generally nonstationary behavior of the observations encountered in real applications, their analysis in time-frequency domain constitutes the most appropriate technique to identify the relevant structures for information processing.

Manuscript received March 10, 2009; accepted February 28, 2010. Date of publication April 12, 2010; date of current version July 14, 2010. The associate editor coordinating the review of this manuscript and approving it for publication was Prof. Haldun M. Ozaktas. The present work was done in collaboration with French DGA (Délégation Générale pour l'Armement) under research Contract CA/2003/06/CMO.

C. Ioana is with the Grenoble INP/GIPSA-lab, 38402 Saint Martin d'Heres, Grenoble, France (e-mail: Cornel.Ioana@gipsa-lab.inpg.fr).

A. Jarrot is with the ENSIETAn Brest, Engineer Etudes et Productions Schlumberger, 92142 Clamart, France (e-mail: jarrotar@ensieta.fr).

C. Gervaise is with the ENSIETA, E3I2 Lab, 29806 Brest, France (e-mail: Cedric.Gervaise@ensieta.fr).

Y. Stéphan is with the Military Oceanography Department, 29200 Brest, France (e-mail: Yann.Stephan@shom.fr).

A. Quinquis is with the Scientific Research and Innovation Division, DET/GESMA BP 42-29240 Brest Armées, France (e-mail: andre.quinquis@dga.defense.gouv.fr).

Color versions of one or more of the figures in this paper are available online at http://ieeexplore.ieee.org.

Digital Object Identifier 10.1109/TSP.2010.2048102

A typical application of time-frequency analysis is the underwater signal processing, due mainly to the nonstationarity of the underwater signals. In this area, considering the dispersive behavior of the underwater channel became very important, especially in the case of underwater systems operating at low frequencies (mainly, below 200 Hz). As we show in this paper, a dispersive channel modifies a transmitted signal in a complex way, introducing multicomponent structures with nonlinear time-frequency shapes. More precisely, a dispersive channel produces different delays of spectral components according to their frequencies: high frequencies propagate faster than the low ones [1]. The transformation of signal propagating in dispersive channel can be characterized by a nonlinear change of the phase function of the signal:$\xi(t/t_r)$ where t_r is the reference time. For example, in shallow water environment, the phase changes according to $\xi\left(t/t_r\right)=\sqrt{\left(t/t_r\right)^2-\left(\alpha/t_r\right)^2}\,(t\gg\alpha;\alpha=R/c)$, where R is the source-receiver range and c is the sound speed in water column [8]. This change is specific to each propagation path. In conclusion, a signal received in a dispersive channel is composed of many components, each one having distinct time-frequency shape according to its propagation mode [1]. In addition, these components are very close in time which makes it difficult to separate them.

The dispersion phenomena occur in different domains such as underwater environment, dielectrics, radio waves in ionosphere, etc. Their analysis could be of great help since the knowledge of dispersion allows understanding the physical phenomena behind the dispersion. Knowing the dispersion behavior of the channel helps improving the efficiency in many applications such as communications, localization, etc.

The main idea, proposed in [2], is to employ matched time-frequency spreading functions that depend on $\xi(t/t_r)$. Using this concept, the output of a dispersive system can be expressed as the superposition of dispersive signal transformations weighted by these matched dispersive spreading functions. In spite of its accuracy, the concept introduced in [2] is difficult to implement in practice since it is based on continuous signal transformations. Discrete formulations have also been proposed based namely on the decomposition of narrowband spreading function into a weighted summation of sampled time-frequency shifts, multiplied by a smoothed discrete version of the spreading function [3]. Recently, the discrete characterization of dispersive time-varying systems has been proposed as the generalization of the discrete narrowband time-frequency model [4]. More precisely, assuming the function $\xi(t/t_r)$, the approach proposed in [4] unifies the

discretization procedure for any dispersive system through unitary warping between narrowband spreading function and the dispersive spreading function. Using this characterization, the authors proposed a time-frequency RAKE receiver exploiting the joint multipath-dispersion diversity. Its successful use for communication over dispersive underwater channel has been proved.

The aforementioned approaches establish a general framework for signal processing in dispersive media. The characterization of such environment in terms of wideband spreading function is very well suited for receiver structure design adapted to dispersive environment. Nevertheless, the accuracy of this characterization depends strongly on the *a priori* information of the phase change, $\xi(t/t_r)$. There are several cases when information on the phase deformation are available. For example, if the geometrical and physical parameters of the channel are known, the phase deformation could be numerically evaluated using the theory of modes [1]. Two cases have been extensively studied in the literature, mainly because they can be analytically modeled: iso-velocity channel (i.e., channel having the same sound velocity over all volume) [1] and Pekeris channel [6]. In other cases, numerical simulations are used to asses physical properties of dispersive channels basically based on the concept of matched-field processing [26]. In operational context, the underwater dispersive channels are estimated using techniques developed in seismic exploration [27]. That is, the channel is estimated by exploring received signals by a sensor network when the wideband signals are transmitted from explosive sources. The inversion is done by processing received data (using wavelet transforms, for example [27]) and referring to the source position which is known. In addition, the inversion is more efficient when the source-receiver range is large since modal arrivals are better separated in time domain.

In passive configurations (i.e., no information available about the source position and transmitted signal), if the channel is unknown and there is no time for its characterization by conventional techniques (bathymetry or multisensor tomography), which could be the case of military operations in shallow water, information about phase changes due to the dispersion are difficult to obtain. In this case, one possible solution is to investigate the channel characteristics by taking advantage of signals propagating in this channel. Hence, *analyzing* precisely the signal received from a dispersive channel could help us to find out information about the phase changes due to the dispersive effects. This information, used in addition with the spread functions-based methods [4], [5], could provide an efficient characterization of dispersive channel in *realistic* (i.e., no *a priori* information available), *general* (performing in any type of dispersive channel) and *operationally blind* (i.e., we can use signal existing in the channel as an echolocation signal, for example) contexts.

In this paper we propose a methodology for estimation of phase change functions $\xi(t/t_r)$ induced, on an arbitrary transmitted signal, by a dispersive channel. Since no *a priori* information on signals is available, the methodology exploits the coherence of fundamental parameters of any type of signals: amplitude, frequency and phase. Specifically, the time-frequency structures of received signal will be separated by analyzing their continuity in terms of instantaneous amplitude, phase, frequency. Since these structures are close (because of the multipath propagation effect) the continuity criteria will be aimed to provide high-resolution capabilities. Furthermore, once the time-frequency structures are estimated, they will be filtered by using the generalized time-frequency filters structures [7]. Finally, individual analysis of each structures and comparison between successive arrivals provide information about phase changes due to the dispersion.

This methodology is demonstrated in the context of underwater dispersive channels. Realistic configurations will be used in order to illustrate the performance of the proposed approach. Although the performance is illustrated in the underwater configuration, the proposed approach is general since it exploits fundamental attributes related to any type of signals (amplitude, phase and frequency).

The paper is organized as follows. In Section II we briefly discuss the problem of signal processing in the context of dispersive propagation channels. In Section III we define the concept of time-frequency-phase continuity and illustrate its benefits on synthetic data. The methodology of dispersive phenomena estimation is introduced in Section IV. The results provided in Section V illustrate the benefits of this concept in the context of underwater blind low-frequency source localization. We conclude in Section VI.

II. Modeling Signal Received From an Underwater Dispersive Channel

The acoustic waves are widely used in underwater channels for communications, detection, localization or estimation of physical properties. The underwater channel provides the best propagation support for acoustic waves but the transmitted signal is often distorted. The distortions are generated by physical parameters of the water column (water density, sound speed profile), parameters of sea bottom (density and sound speed of seabed layers, attenuation coefficients, etc.), geometrical parameters (depth, bathymetry). These distortions have to be considered in order to ensure satisfactory receiving performances.

The parameters of the transmitted signal are chosen according to the operational purposes of the system. Hence, the central frequency of the spectrum depends on the required transmission ranges. In this paper, we address the problem of signal analysis in the context of long-range communications in shallow water medium. Under these conditions, one mathematical solution for modeling the propagation phenomena is the theory of modes [9]. According to this theory, the transfer function of the underwater acoustic channel defined between a transmitter located at $(0, z_s)$ and a receiver located at (r, z_r) (Fig. 1) can be expressed (after few simplifications related to boundary conditions) as

$$H(f) = \sum_{m=1}^{+\infty} g_m(z_s)\, g_m(z_r)\, \frac{\exp(-jk_r(m,f)\, r)}{\sqrt{k_r(m,f)\, r}} \qquad (1)$$

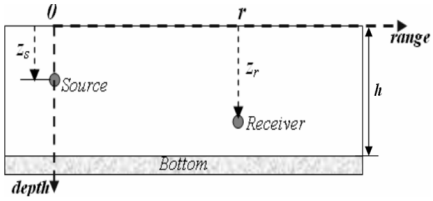

Fig. 1. Configuration source-receiver in an underwater environment.

where $k_r(m,f)$ are the horizontal wavenumbers, g_m are the modal functions (or Green functions) of index m and they are solutions of the equation:

$$\frac{\partial^2 g}{\partial z^2} + \left(\left(\frac{2\pi f}{c(z)} \right)^2 - k_r^2(m,f) \right) g = 0 \tag{2}$$

where $c(z)$ is the sound speed profile.

The expression (1) can be written, in a simplified form, as:

$$H(f) \approx \sum_{m=1}^{+\infty} \frac{A(m,f)}{\sqrt{r}} \exp\{jk_r(m,f)\, r\}. \tag{3}$$

This expression states clearly that the transfer function of a dispersive underwater channel has a multicomponent structure, each component being defined by its wavenumber and frequency. The term $A(m,f))/\sqrt{r}$ represents the attenuation rate of corresponding component. It depends on the modal functions corresponding to the transmitter and receiver depths (1), to the wavenumber and to the range between transmitter and the receiver. The response of this component to one monochromatic signal, $\exp(j2\pi f_0 t)$, can be written as

$$s_m(t) \approx D(m,f_0) \exp\left(j2\pi f_0 t - jk_r(m,f_0)\, r\right). \tag{4}$$

The mth-order component of the transfer function produces, when the input is a monochromatic signal, a signal similar to one wave traveling from transmitter to receiver. Its wavenumber is $k_r(m,f_0)$ and the expression (4) allows us to define the phase and group velocities [6]:

$$\begin{aligned} v_\varphi(m,f) &= \frac{2\pi f}{k_r(m,f)} \\ v_g(m,f) &= 2\pi \frac{\partial f}{\partial k_r(m,f)}. \end{aligned} \tag{5}$$

As indicated in [9], the wavenumber $k_r(m,f)$ is "responsible" for the dispersion phenomena. More precisely, for distinct index m and, at the same frequency f, the arrivals of modes. mth will have different phase and group velocities. This phenomenon is called *intermodal dispersion*. On the other hand, in the case of a single mth-order component, the wavenumber is frequency dependent. This is called *intramodal dispersion*. Under these considerations and using the (4) and (5) we can define the channel impulse response as follows:

$$IR(t,f) = \sum_m D(m,f)\, \delta\left(t - \frac{r}{v_g(m,f)}, f \right). \tag{6}$$

A quadratic time-frequency representation of the channel impulse response (Wigner–Ville distribution, for example) leads to the following expression:

$$\begin{aligned} \text{TFR\_S}(t,f) = &\sum_m D(m,f)\, \text{TFR\_I}\left(t - \frac{r}{v_g(m,f)}, f \right) \\ &+ \sum_i \sum_j D(i,f)\, D(j,f)\, \text{TFR\_I}\left(t - \frac{r}{v_g(i,f)}, f \right) \\ &\times \text{TFR\_I}\left(t - \frac{r}{v_g(j,f)}, f \right) \end{aligned} \tag{7}$$

where TFR_I is the time-frequency representation of the transmitted (or input) signal.

This expression can be interpreted as follows: one source transmitting energy at t_0 and with frequency f_0 will be transformed, via the propagation in a channel defined by (6), in a set of energy packets arriving at $t_0 + r/v_g(m,f_0)$ and weighted by $D(m,f_0)$.

The expression (7) shows the complexity of the received signal in a dispersive channel. Hence, even if a simple signal is transmitted, the propagation will introduce both frequency-dependent and propagation path-dependent attenuations and delays. These produce a nonlinear time-frequency deformation, specific for each propagation path. To illustrate these phenomena we consider an iso-velocity underwater channel with a rigid bottom. The depth of water column is h and sound velocity, constant over all channel, is c. Such a channel is illustrated in Fig. 1 and its choice is motivated by the fact that only iso-velocity channels are characterized by analytical solutions of the propagation equation [9].

Under these assumption, the expressions of the wavenumber and group velocity are

$$k_r(m+1,f) = \sqrt{\left(\frac{2\pi f}{c} \right)^2 - \left[(2m+1)\, \frac{\pi}{2h} \right]^2} \tag{8a}$$

$$v_g(m,f) = \frac{c^2}{2\pi f} \sqrt{\left(\frac{2\pi f}{c} \right)^2 - \left[(m-0.5)\, \frac{\pi}{h} \right]^2}. \tag{8b}$$

The expression (8a) shows that, for a given frequency f, if $m \geq 2hf/c - 0.5$, the wavenumber, k_r, can have imaginary values. This corresponds to strongly attenuated modes.

The group velocity depends on the frequency, f and on the mode number, m as shown in (8b). For high-order modes, the waves are slow at a given frequency (intermode dispersion effect). Otherwise, for a given mode, the wave velocity increases with the frequency (intramode dispersion effect).

These (8a) and (8b) are evaluated in the case of an iso-velocity waveguide of depth $h = 16$ m and for a source and receiver located at 4 m depth. The source–receiver range is 2000 m. Fig. 2 displays the impulse response of this channel. The dispersion phenomenon is visible especially to the low frequencies [Fig. 2(a)]. Fig. 2(b) shows the received signal propagated by this channel when the transmitted signal is a chirp with the following parameters: duration, 1s; $f_{\text{start}} = 0$ Hz; $f_{\text{stop}} = 1000$ Hz. As we can remark on this picture the high frequencies arrive firstly as well as the modes with small indexes m.

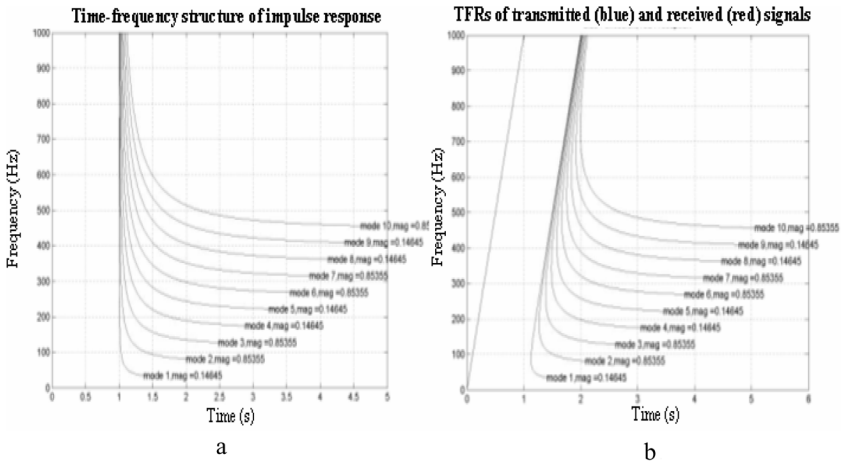

Fig. 2. Time-frequency representations of the impulse response of an isoceler dispersive channel (a) and the received signal from this channel (b).

The results illustrated in Fig. 2 confirm the theoretical statements presented above. They are available for iso-velocity waveguides which constitute the simplest case. If the sound speed profile is arbitrary the dispersion effect is much more complex and no analytical model can be formulated. In terms of signal analysis, even this simplest case illustrates the difficulties arising from dispersion effect. If the chirp is used as the transmitted waveform of an underwater positioning system, for example, the dispersion avoids using of match filtering of received signal: the efficiency of this traditional processing tool is affected by the time-frequency composition changing due to the dispersion [Fig. 2(a)]. Some physical assumptions concerning the channel seem to be necessary if the optimal processing (in the sense of match filtering) is required.

The aim of the Sections III–V is to propose a methodology for characterizing the time-frequency content of the dispersive arrivals. This information is essential to asses the physical behavior of the channel.

III. The Concept of Time-Frequency-Phase Continuity

As indicated in the previous section, the signal issued from a dispersive channel contains several nonlinear time-frequency structures having different laws strongly related to the physical properties of the channel. In real configuration, the assumptions necessary to assess physical considerations about the channel are difficult to make. The approach proposed in this paper provides information about physical considerations by processing **only** the received signal. Taking into account the nonstationarity of the signal, the time-frequency analysis seems to be an appropriate processing tool. The spectrogram of the first four modes defined in Fig. 2 is illustrated in Fig. 3.

As shown by Fig. 3, identifying the four components is not a simple task. The linear representation [Fig. 3(a)] shows only two modes the other two being invisible because of their much smaller energies with respect of strongest ones. One can use a logarithmic representation [Fig. 3(b)], with the price to pay being the poorer resolution. For these reasons, the extraction of each individual mode could be a complex problem.

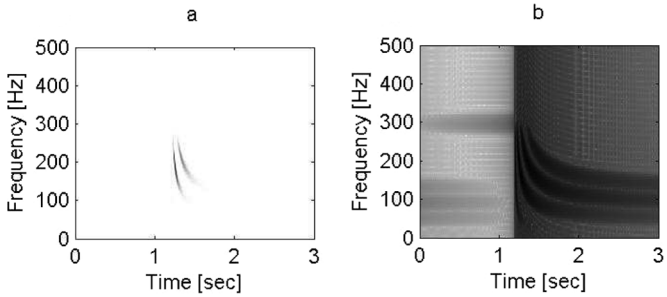

Fig. 3. Spectrogram of the first four modes defined in Fig. 2(a). (a) Magnitude of spectrogram. (b) Log magnitude of spectrogram.

More generally, the extraction of nonlinear time-frequency structures is an active area of research in the field of time-frequency analysis. The problem becomes very complex if no *a priori* information about the analyzed signal are available. This is actually the case considered in this paper: the aim is to identify the dispersive behavior of underwater channel considering, as observing data, the signals issued from this channel corresponding to an impulsive transmitting signal. As indicated in Fig. 3, the time-frequency analysis context is complex even in the case of a synthetic data. That is, the time-frequency structures are nonlinear (with distinct shape) and they are very close, very often out of the resolution limits of well known time-frequency distribution. In [4] and [5], the authors proposed a physical driven algorithm for mode extraction in a dispersive channel. Hence, the idea is to assume a given physical model of the channel parameterized by some unknown parameters that have to be estimated. Furthermore, using some warping-based time-frequency representations (parameterized by set of possible values of channel's parameters) of the received signals, the best stationarization will correspond to the channel's parameters closest to real configuration. This interesting methodology can provide an optimal result if a large set of channel's parameters is tested in order to find the best solution.

One alternative solution, avoiding considering a large number of parameters values, is to look for the coherence of fundamental signal's parameters: instantaneous amplitude, frequency

and initial phase. Assuming that each signal's time-frequency structure could be modeled, in accordance with the Weierstrass theorem, by mean of a polynomial function, the model of received signals is expressed as

$$x(t) = \sum_{i=1}^{N} A_i(t)\, e^{j\phi_i(t)} + n(t) \tag{9}$$

where: $x(t)$ is the received signal composed by N components, $A_i(t)$ is the amplitude envelope of ith component (considered slowly varying with respect of instantaeous phase), $\phi_i(t)$ is the time-varying phase of ith component and n is the noise. In the case of signals issued from an ideal dispersive channel, the phase of one component is expressed with (4). In the general case of arbitrary channels, an analytic expression does not exist. In this section, we define a general framework which is aimed to provide an estimation of the phase function of each component knowing that the phase $\phi_i(t)$ does not admit any analytical form.

The estimation of the phase function of ith component can be expressed as a maximum-likelihood estimation problem. Let H_0 and $H1$ be defined by

$$\begin{cases} H_0 : x(t) = n(t) & \text{Noise only} \\ H_1 : x(t) = A_i(t)\, e^{j(\phi_i(t)+\varphi_i)} + n(t) & \text{Signal and noise} \end{cases} \tag{10}$$

where φ_i is the initial phase and $A_i(t)$ is the amplitude modulation law, supposed slowly varying in comparison with the instantaneous phase low, $\phi_i(t)$. Here, H_0 represents the case when the received signal contains no signal and H_1 represents the case when the received signal contains at least the ith component. In such a case, all the components different from ith are considered as noise. Thus, a possible solution to find the estimated phase law $\tilde{\phi}_i(t)$ that best matches the true phase law $\phi_i(t)$ consists to maximize the log-likelihood ratio defined as

$$\tilde{\phi}_i(t) = \underset{\phi_i(t),A,\varphi_i}{\operatorname{Argmax}} \ln \frac{f(x|H_1)}{f(x|H_0)} \tag{11}$$

between the statistics $f(x|H_0)$ and $f(x|H_1)$ of H_0 and H_1, respectively. In order to make the maximization independent of the two parameters A, φ_i a possible solution consists to replace the maximum-likelihood estimation of each unknown quantities assuming that all other parameters are known. This approach, called generalized maximum likelihood [10], gives for the estimation of A, φ_i(K—the number of samples)

$$\tilde{A}_i = \frac{\left(\sum_{k=1}^{K} x[k]\cos(\phi_i[k]+\varphi_i)\right)^2}{2\sum_{k=1}^{K}\cos^2(\phi_i[k]+\varphi_i)} \tag{12}$$

and

$$\tilde{\varphi}_i = \angle\left(\sum_{k=1}^{K}\sum_{l=1}^{K} x[k]\cos(\phi_i[l])\sin(\phi_i[k]-\phi_i[l]) + i\sum_{k=1}^{K}\sum_{l=1}^{K} x[k]\sin(\phi_i[l])\sin(\phi_i[k]-\phi_i[l])\right) \tag{13}$$

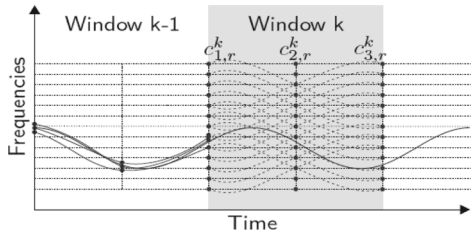

Fig. 4. Illustration of the exhaustive search procedure.

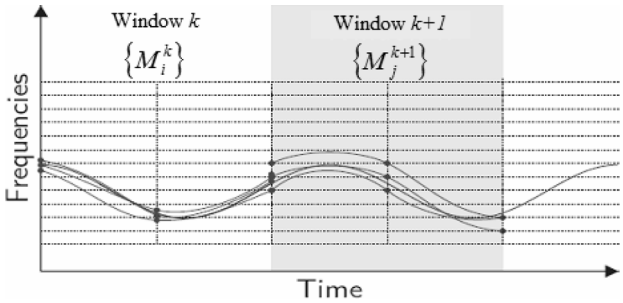

Fig. 5. Exhaustive searching and optimization results.

where $\angle a + ib$ denotes the complex angle of $a + ib$.

However, this approach remains difficult to solve by direct computation. For this reason we shall restrict ourselves to an exhaustive search of the best phase estimate. Because of the extreme variability of $\tilde{\phi}_i(t)$, an exhaustive search over all time-frequency pairs is not computationally viable. Our strategy consists in performing an exhaustive search over a local but general model of the instantaneous phase. Hence, we carry out the processing over a time window. This is illustrated in Fig. 4 where the characterization of an arbitrary time-frequency component (solid line) is considered.

As indicated in Fig. 4, in each window, a set of time-frequency component is constructed for different nodes (i.e., a node is defined by a pair of time and frequency coordinates) over a grid parameter. For each component, the log-likelihood is estimated over the window and a finite number of components, i, giving highest likelihood is selected. Let us denote a component over the window k as M_i^k. Then, in order to optimize the value of the selected nodes, an optimization is performed using a simplex method [11] with the selected time-frequency points as initialization. The result obtained after this step is illustrated in Fig. 5.

The next step consists of regrouping the detected components. Since each component M_i^k represents a local model, the goal of this regrouping step is to find the values of M_i^k, $k = 1, 2, \ldots, K$ that best represents the original component i with respect to the maximum-likelihood criterion. Hence, our strategy consists of associating two components from two adjacent windows (k and $k+1$), M_i^k and M_j^{k+1}, if they satisfy some time-frequency-phase coherence criteria. Four such criteria are defined.

1) c^0 time-frequency continuity. This criterion is given by $C^0\left(M_i^k, M_i^{k+1}\right) = \left|f_f\left(M_i^k\right) - f_i\left(M_j^{k+1}\right)\right|$ where $f_i\left(M_j^{j+1}\right)$ is the initial frequency of component M_j^{k+1} and $f_f\left(M_i^k\right)$ is the final frequency of component M_i^k.

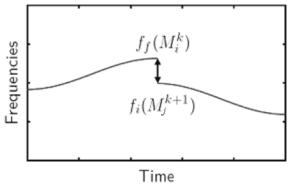

Fig. 6. C^0 time-frequency continuity.

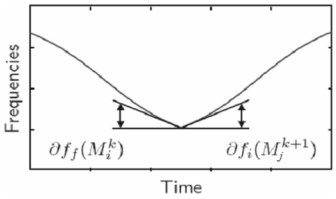

Fig. 7. C^1 time-frequency continuity.

This criterion is based on the frequency discontinuities between the component M_i^k and M_j^{k+1} (Fig. 6). For example, if $C^0\left(M_i^k, M_j^{k+1}\right)$ has high value, the probability that M_i^k and M_j^{k+1} belong to the same time-frequency component is low.

2) C^1 time-frequency continuity. This criterion is given by $C^1\left(M_i^k, M_j^{k+1}\right) = \left|\partial f_f\left(M_i^k\right) - \partial f_i\left(M_j^{k+1}\right)\right|$ where $\partial f_i\left(M_j^{k+1}\right)$ and $\partial f_f\left(M_i^k\right)$, respectively, denote the initial and final instantaneous frequency rates of the components M_j^{k+1} and M_i^k. As indicated by Fig. 7, this criterion rules the connection of M_i^k and M_j^{k+1} in the following way if the rates of IFLs are almost the same the time-frequency content variation is smooth being subject to a single component (Fig. 7). In this case, M_i^k and M_j^{k+1} are merged. If the rates are too different, then both components do not belong to the same structure.
3) Amplitude continuity. This criterion is given by $dA\left(M_i^k, M_j^{k+1}\right) = \left|A\left(M_i^k\right) - A\left(M_j^{k+1}\right)\right|$ where $A\left(M_i^k\right)$ denote the maximum-likelihood amplitude of M_i^k estimated by (12). This criterion reflects the general observation that the energy of a time-frequency component varies slowly.
4) Instantaneous phase continuity. The criteria is given by $d\phi\left(M_i^k, M_j^{k+1}\right) = \left|\angle\cos\left(\phi_f\left(M_i^k\right) - \phi_i\left(M_j^{k+1}\right)\right) i\sin\left(\phi_f\left(M_i^k\right) - \phi_i\left(M_j^{k+1}\right)\right)\right|$ where $\phi_i\left(M_j^{k+1}\right)$ and $\phi_f\left(M_i^k\right)$ respectively denote initial and final instantaneous phases, estimated by (13). This criterion merges two candidate components if the phase is continuous.

With these criteria, we define the penalty function of two components estimated from two adjacent windows by

$$p(M_i^k, M_j^{k+1}) = \alpha C^0\left(M_i^k, M_j^{k+1}\right) + \beta dA\left(M_i^k, M_j^{k+1}\right) + \\ + \gamma C^1\left(M_i^k, M_j^{k+1}\right) | + \delta d\phi\left(M_i^k, M_j^{k+1}\right) \quad (14)$$

where the coefficients $\alpha, \beta, \gamma, \delta$ are the weights for each criteria. The regrouping strategy consists of searching over all the possible values M_i^k, $k = 1, \ldots, K$ to find the M_i^k that minimizes the penalty function based on these four criteria

$$p_{opti} = \arg\min \sum_k p(M_i^k, M_j^{k+1}). \quad (15)$$

The minimization of this penalty function enables us to extract individual time-frequency structures. This information will be used in order to filter out time-frequency signal's components as discussed in Section V.

IV. Methodology of Dispersive Phenomena Estimation

The goal of the method introduced in this section (Fig. 8) is to perform the iterative extraction of each component of a signal modeled by (9). At the first iteration, the time-frequency-phase criteria introduced previously provides the time-frequency region occupied by the most energetic component. Once this region estimated, we use a nonstationary time-frequency filter in order to physically extract the signal bounded by this region [7].

Once the extraction has been performed by filtering out the corresponding component, the residual is analyzed with the same time-frequency-phase criteria. This step is iterated i times in order to extract other time-frequency components.

We illustrate the steps of this algorithm using the signal defined in (16) and (17). The synthetic signal is composed of two components having different IFLs: sinusoidal frequency modulation and fourth-order polynomial phase modulation:

$$s(t) = a_1(t)\, e^{j2\pi[0.3t + (10/\pi)\sin(2\pi t \cdot 0.001t)]} \\ + a_2(t)\, e^{j2\pi\left[0.25t - 7.45\cdot 10^{-11}\cdot(t-512)^4\right]} \\ t = 0 \ldots 1023 \quad (16)$$

where $a_1(t)$ and $a_2(t)$ are the amplitude variations of the two components. Two cases will be considered in our simulations:

$$\text{Without modulation: } a_1(t) = 2; a_2(t) = 1 \\ \text{With modulation: } a_1(t) = 2 - 9.75\cdot 10^{-4} t; \\ a_2(t) = 0.3 + 2.9\cdot 10^{-3} t. \quad (17)$$

The IFLs and the amplitude variations (for the second case) are represented in Fig. 9(a). We remark the nonlinear shape of the time-frequency content of the signal. Its analysis, using quadratic time-frequency distributions belonging to Cohen's class, is subject to some limitations related to the trade-off between resolution and interferences terms (both inner, due to the nonlinearity of the time-frequency content, and cross terms), as indicated in Fig. 9(b), where smoothed pseudo-Wigner distribution has been used (the window used is Kaiser). In the context of inherent limitations of the linear or quadratic TFR, the estimation of instantaneous frequency laws of such signals is, since the 1990s, a field of high interest for signal processing community. A first concept that deals with such problem has been developed from the Wigner–Ville distribution as an extension of this well known method to polynomial phase signals (PPS). Hence, the polynomial Wigner–Ville distribution has been introduced as an appropriate method for analyzing the PPSs [13]. Other techniques have been developed, attempting

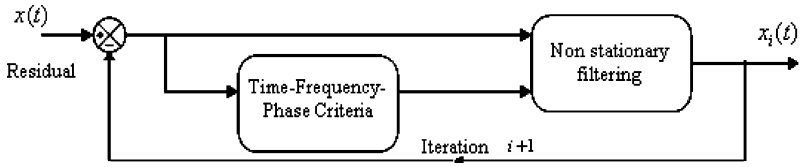

Fig. 8. Method for component extraction.

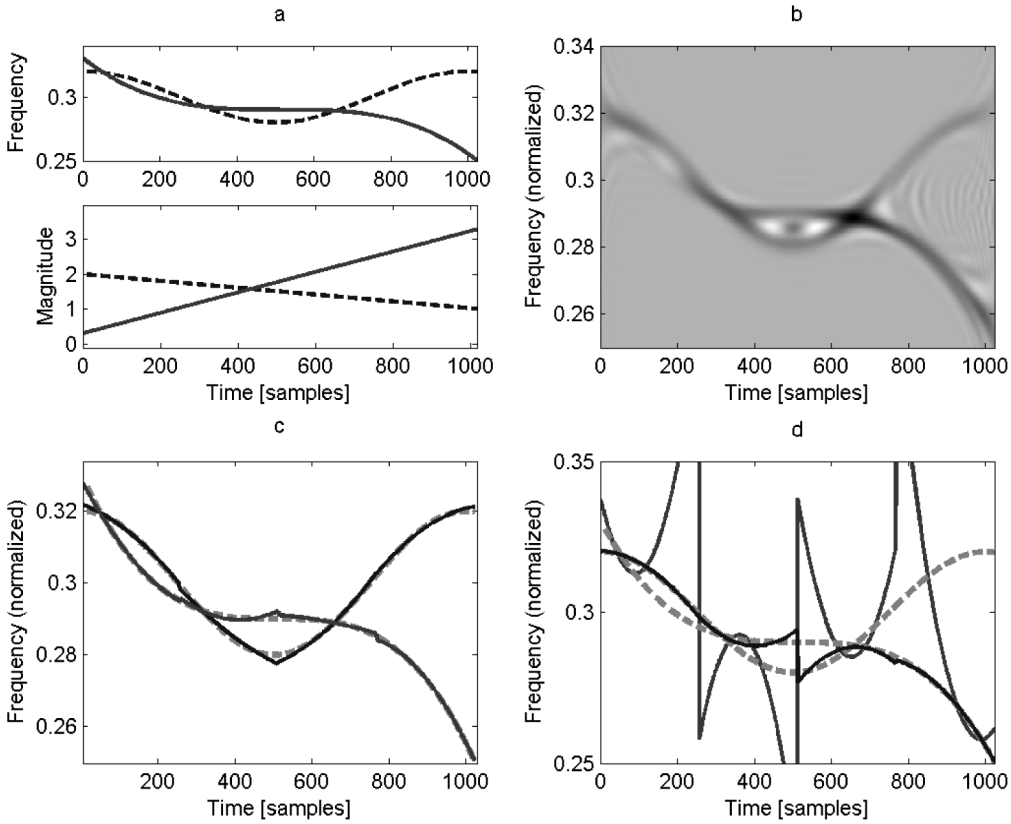

Fig. 9. Synthetic signal and its time-frequency characterization using smoothed pseudo-Wigner distribution and PHAF results. (a) Theoretical IFLs and amplitude modulations of the analyzed signal. (b) SPWD of synthetic signal (c) PHAF estimation-without amplitude modulations. (d) PHAF estimation-without amplitude modulations.

to adapt the polynomial TFR for multicomponent signals [14] or to improve its robustness in noise conditions [15]. The multicomponent signals and the concentration of the polynomial TFR are still current problems, and many researchers focus on them.

Another class of time-frequency techniques devoted to nonlinear T-F contents is based on a warping operator [18], [19]. However, in the context of the polynomial phase signals, these techniques are not always easy to apply while they require that the instantaneous phase be an invertible function (for warping operator design).

The parametric characterization of the polynomial phase signals has been developed around the concept of *high-order ambiguity function* (HAF) [16]. The instantaneous phase of a signal is estimated by a polynomial whose coefficients are calculated from the maximum values of the HAF. The main problems of the HAF are related to the multicomponent signals and noise robustness. A powerful solution has been proposed in 1998 by Barbarosa and his collaborators [17], and it combines the HAFs evaluated for several sets of lags. The product of these HAFs [which gives the bale of the method—product high order ambiguity function (PHAF)] provides high noise robustness and good capabilities for multicomponent signals. For these reasons, this method will be compared with the method proposed in this paper.

The concepts of polynomial TFRs are generally limited in the context of high-order polynomial instantaneous phase. Therefore, the short-time polynomial TFR constitutes the general solution for the estimation of the instantaneous phase requiring high-order polynomials. Such strategy is indicated for synthetic signal used in our simulations as shown in Fig. 9(c): the short-time third-order PHAF has been applied in a window of 256 points. We remark that the estimated IFLs (solid curves) are close to the theoretical IFLs (indicated by dashed curves). To deal with the multicomponent structure of the test signal, the PHAF-based procedure is as follows: in a given window, the IFL of the most energetic cubic FM is estimated and then subtracted before the estimation of the second component.

As indicated in Fig. 9(c), the PHAF-based method provides accurate IFL estimations in the case of two PPS with constant

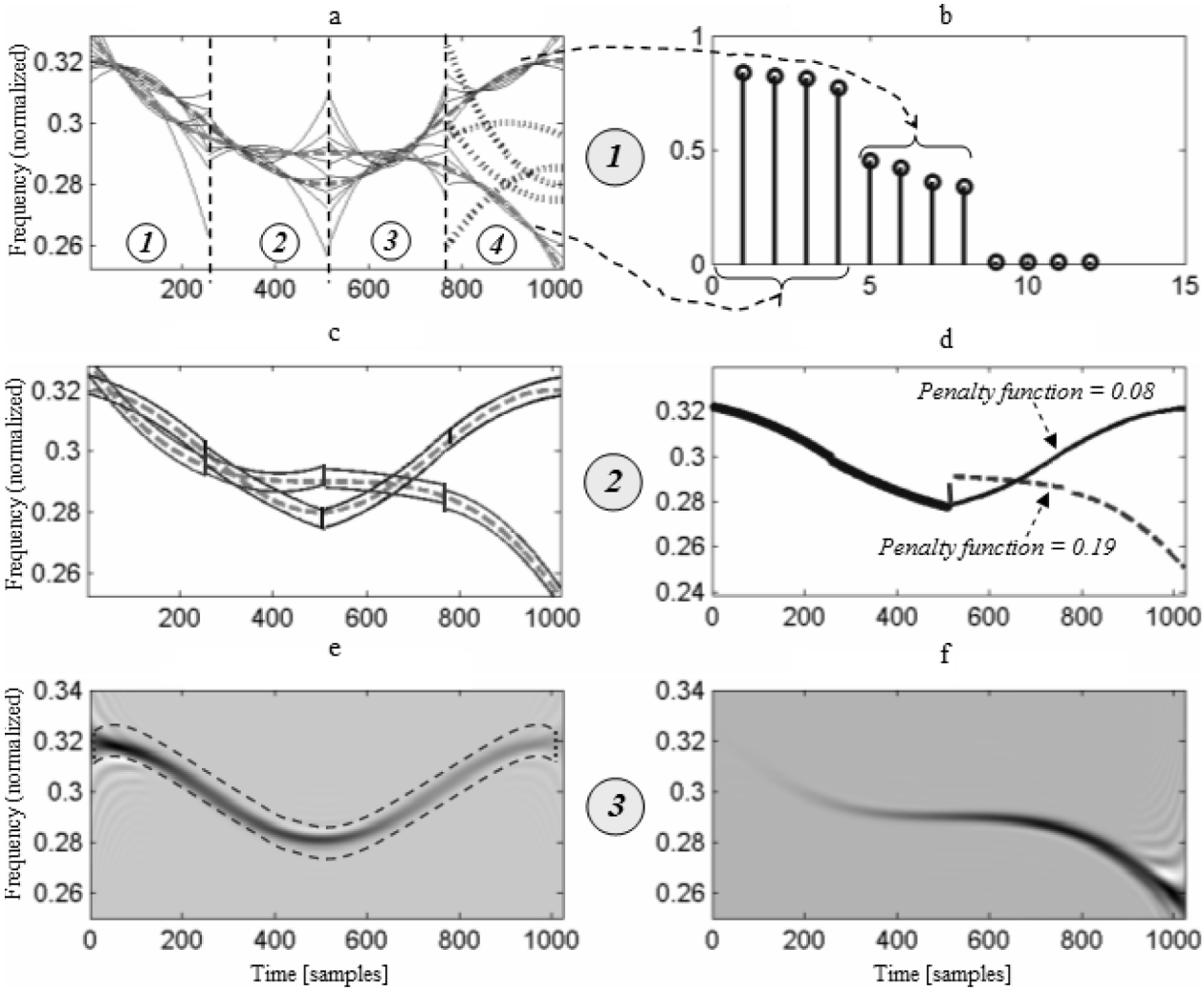

Fig. 10. Organization of the IFL estimation method proposed in this paper. (a) Short time projection on cubic FMs. (b) Correlation coefficients. (c) Short-time T-F filters. (d) Two candidate T-F paths. (e) First extracted component. (f) Second extracted component.

amplitudes (without amplitude modulations). The efficiency decreases when the signal's components have varying amplitudes [Fig. 9(a)]. This is shown in Fig. 9(d). where we remark that, in each window, only the most energetic component is relatively well estimated. After the subtraction, its amplitude modulation is still present and, consequently, the estimation of the second component is considerably affected [Fig. 9(d)]. Actually, while the amplitude modulations are not taken into account (by this version of PHAF-based IFL estimation), the PHAF models the interferences between the second component and the amplitude variation of the first one. Another consequence is the interpretation of the short-time IFL modeling. As it is shown in Fig. 9(d), because of the amplitude variations, the first half part of sinusoidal modulation and the last half part of fourth-order PPS are well estimated. An eventual fusion of the short-time modeled IFLs would lead to a wrong time-frequency structure (solid blue curve).

In order to avoid these problems related to polynomial phase modeling, the methodology based on time-frequency-phase continuity is introduced, providing, as we show in the following, more flexibility for signals with both amplitude and nonlinear frequency modulations.

The first step of this methodology consists of partitioning the signal into a given number of analysis windows [Fig. 10(a)]. In the ith window, we define a set of third-order frequency modulations (cubic FM) $\left\{M_k^i\right\}$ with $k = 1, \ldots, P$ P is the number of components). From this set of components, we will retain the K most correlated cubic FMs with the signal samples corresponding to the considered window. For the analysis done in the fourth window, the correlation coefficients with several cubic FMs are plotted in Fig. 10(b). We observe that there are three groups of coefficients. The first one correspond to the correlation with the signal's part associated to the four-order PPS that, for the considered window (fourth one), is the most energetic. This leads to strong correlation coefficients. The second group of correlation coefficients [Fig. 10(b)] corresponds to the correlation with cubic FMs modeling, in the fourth window, the sinusoidal frequency modulation. While this component of the signal (equations (16)–(17)) is weaker, the corresponding coefficients are smaller than previous ones. Finally, we illustrate, in Fig. 10(b), the third group of the coefficients which are very small: they correspond to the correlation with other cubic FMs [dashed curves in Fig. 10(a)] that are not similar to any component of analyzed signal. The small values of the correlation

coefficients indicate that the corresponding cubic FMs cannot be included in the retained set of cubic FM .

For each time-frequency curve corresponding to the set of cubic FMs $\left\{M_k^i\right\}$ with $k = 1, \ldots, K$ obtained in the first step (Fig. 10), we design a time-frequency filter [7], [20] which is aimed to extract the samples corresponding to time-frequency content of the signal. The local time-frequency filters, for the most correlated cubic FMs with the both signal's component, are plotted in Fig. 10(c) (for simplicity reasons, we plot only two filters per analyzing window knowing that, for each window, K filters are designed). The signal obtained from each local time-frequency filtering is used to compute, via (12)–(13), the instantaneous amplitude and phase, respectively. The computation of time-frequency-phase criteria (see the previous section) is done between all instantaneous phases of adjacent window. Therefore, different time-frequency paths are obtained each one having a given value of penalty function. For our example, we consider two paths composed, between in the interval 1–512 samples, by the same time-frequency structure and, after the sample 512, by the two paths represented in Fig. 10(d). The path, represented by dashed curve [Fig. 10(d)], corresponds to stronger correlation coefficients [Fig. 10(b)] while the path plotted by solid curve correspond to the weaker correlation coefficients. Despite the difference between correlation coefficients, the penalty function is smaller in the case of the path represented by a solid curve. The penalty function we used is composed only of C^0 criterion with a weight of 10. More precisely, we strongly penalize the discontinuity of IFLs as shown in Fig. 10(d). The transition from IFL corresponding to [0,512] samples to the IFL represented by dashed curve is highly penalized which avoid the fusion of the mentioned path. In conclusion, the minimization of global penalty function ensures, in the second step, the modeling of one of the signal's time-frequency structure. Off course, according to the signal's type, the criteria should be differently defined. For example, in the case of FSK signals, the initial phase continuity criterion should be used with the highest weight. In our case, while we assume that we deal with continuous IFLs, the choice of the C^0 criterion is adopted.

The estimated IFL, obtained from the minimization of the penalty function, is used, in the third step, to design the global time-frequency filter that will extract the corresponding component of the signal. For the test signal, the global time-frequency filter designed from the path previously estimated [Fig. 10(d)] accurately extracts the sinusoidal frequency modulation [Fig. 10(e); the filter is plotted with dashed curve]. After the extraction of this component, reapplying the procedure (according to the iterative algorithm defined in Fig. 8) the second component is also extracted [Fig. 10(f)]. Off course, the amplitude modulations will not be exactly reproduced (because of the crossing or of the filtering effects) but they are still visible. In addition, the IFLs are accurately estimated.

In order to quantitatively measure these performances, with respect of existing polynomial modeling tools, the next part of this section is devoted to the comparisons with multi lag HAF (introduced by Peleg and Friedlander [21]) and PHAF. As comparison parameter, we choose the IFL estimation error $(\mathrm{IFL}_E E)$ defined as the L_2-norm of the differences between the theoretical (IFL_t) and estimated (IFL_e) IFLs, respectively

$$\mathrm{IFL\_EE} = \left|\left|\mathrm{IFL}_t - \mathrm{IFL}_e\right|\right|_2 . \tag{18}$$

As an example, a $\mathrm{IFL}_{\mathrm{EE}}$ value of .074 corresponds to an estimation illustrated in Fig. 9(d) while an error of 0.016 is equivalent to the case illustrated in Fig. 9(c).

The first simulation consists of studying the $\mathrm{IFL}_{\mathrm{EE}}$ obtained for different window sizes. As a test signal we used the sinusoidal FM defined by (16). While the estimation methods are locally applied, this type of analysis could be useful for identifying the "optimal" size of the analyzing window or to establish a multitaper strategy, as suggested, for example, in [22]. The window sizes are variable between 160 and 360 points, with a step of 10 points.

As indicated in Fig. 11(a), for the three methods, some values of window's size minimize the IFL error. Hence, a window size between 210 and 280 points leads to a minimum error of IFL estimation. If the window size exceeds these values, the time-frequency content inside the window is too nonlinear and the modeling using cubic FMs becomes subject of increasing errors. If the window size is below 200 points, the errors increase while the numbers of samples decreases affecting the consistency of HAF's estimator or of the correlation (in the case of the proposed method). In conclusion, for this type of signal, a window size around 260 samples represents the best choice. In our computation, we considered size of 256 samples (dyadic size, interesting for fast computing reasons).

The second simulation set deals with the noise robustness study considering the sinusoidal frequency modulation (equation (16); the amplitude is considered constant) corrupted by an additive white Gaussian noise with a signal-to-noise ratio (SNR) between 0 and 15 dB. For each SNR value, 200 realizations have been used to evaluate the $\mathrm{IFL}_{\mathrm{EE}}$. Fig. 11(b) indicates that the PHAF and the proposed method have similar performance for SNR larger than 5 dB. Below this value, thanks to the projection technique on a large dictionary of cubic FMs, the proposed method performs sensibly better, having a smaller IFL error.

The third simulation set consists of evaluating the IFL estimation accuracy when a two component signal with amplitude modulations is considered. The test signal is the one defined in (16), but the amplitude modulations are characterized by two polynomials of order three with different coefficients. These coefficients are chosen, for each realization, under the constraint of a given ratio between the maximal and minimal amplitude $(A_{\max}/A_{\min})$. In our simulation, this ratio was variable between 1 and 5 with a step of 0.5.

Fig. 11(c) shows that, for the first component (the sinusoidal frequency modulation), the PHAF and the proposed method have similar performances: the IFL estimation error decreases while the $A_{\max}/A_{\min}$ ratio becomes larger. Indeed, compared with the case of ml-HAF, the estimation error increases slowly (almost linearly). Nevertheless, the differences between PHAF and the proposed method become significant in the case of the second component [Fig. 11(d)]. In the case of the PHAF, the reduction of the first component is not accurately done for high

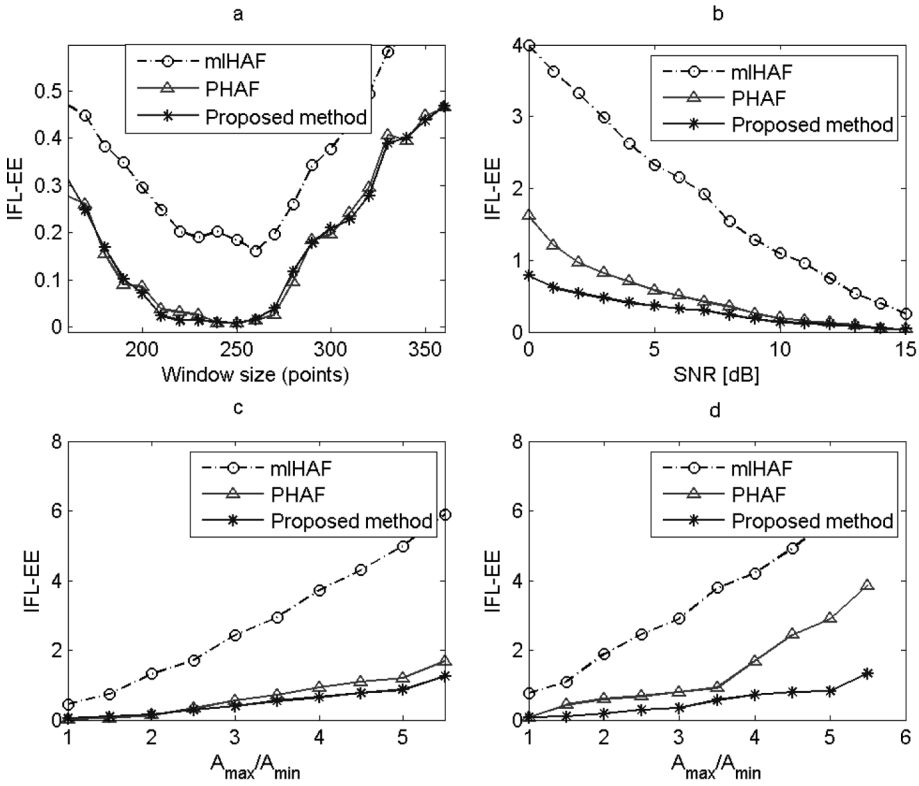

Fig. 11. Comparisons between ml-HAF (of order 3), PHAF-based approach (of order 3) and the proposed method. (a) $\mathrm{IFL_{EE}}$ versus window size. (b) IFL-EE versus SNR. (c) First component: IFL-EE versus $A_{\max}/A_{\min}$ (d) Second component: IFL-EE versus $A_{\max}/A_{\min}$.

$A_{\max}/A_{\min}$ ratio [as illustrated in Fig. 9(d)]. Thus, the estimation of the second component will be blurred by the residuals of the first component. This effect does not exist in the case of the proposed method, thanks to the fusion of short-term cubic FMs which is based on the minimizing the time-frequency-phase continuity criteria.

In conclusion, a general remark is that the both PHAF and proposed method perform, in all simulation contexts, better than the ml-HAF-based approach. Concerning the PHAF technique and the proposed method, we remark that the time-frequency-phase based approach provides, with respect of short-time PHAF, more flexibility and accuracy in estimating the complex IFLs with varying amplitudes. The "price" to pay is the computational complexity which is higher than in the case of PHAF (the computational time is, in average, four times higher in the case of the proposed method). While the IFL estimation results, in simple cases, provided by PHAF and by the proposed method are similar, one idea will be to combine the projection technique and the PHAF in order to achieve good performances in complex situations (high nonlinear IFLs with varying amplitudes) and to decrease the computational complexity.

In the last part of this section, we illustrate the proposed method for the signal defined in Fig. 3. At the first iteration of the method (Fig. 8), the fusion of the local most matched cubic FMs provides a time-frequency shape corresponding to the third modal arrival [Fig. 12(a)]. The size of the window is of 270 samples and it has chosen from several experiences. Actually, a smaller window introduces errors while the correlations between the signal and cubic frequency modulation become weak. Alternatively, a large window would require a higher order for polynomial modeling. Therefore, a window size around 270 samples provides, for this type of signal, the best tradeoff.

The extracted time-frequency structure corresponding to the third mode allows us to define a time-frequency filter [Fig. 12(a)] which extracts the corresponding signal [Fig. 12(b)]. The spectrogram of residual signal is illustrated in Fig. 12(c).

The extraction of the modes is done according to the diagram presented in Fig. 8. The time-frequency-phase criteria provide the time-frequency shape of the most energetic component of the signal. Furthermore, this shape produces the time-frequency filter which physically extracts the component. This is actually the novelty of the proposed methodology with respect of Matching Pursuit-based approaches which performs the component extraction via a subtraction. While this operation requires the estimation of component's magnitude (which is not always an easy task), the method proposed in this paper performs component's extraction via a time-frequency filtering procedure. In this way, the extraction is independent of component's amplitude.

In our example, Fig. 12 shows how the modal arrivals are iteratively extracted. We remark that the time-frequency-phase criteria provide an accurate estimation of time-frequency structures of the signal. The time-frequency filters designed from this estimation [Fig. 12(a), (d), (g)] allow extracting accurately the modal arrivals [Fig. 12(b), (e), (h) and (i)]. After second iteration, one can observe that the filtering-based extraction high-

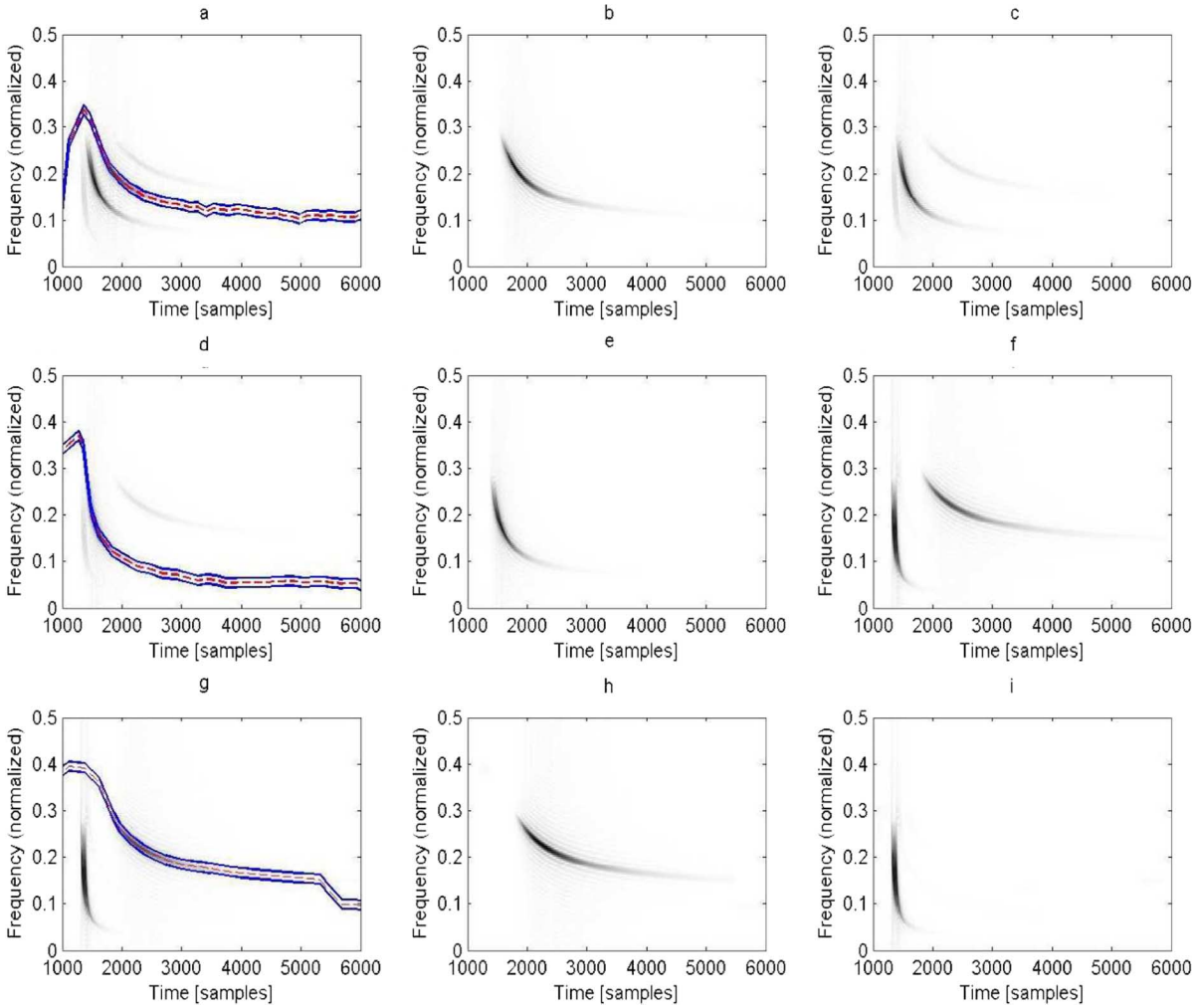

Fig. 12. Extraction of the third-order mode from the signal defined in Fig. 3(a). (a) Time-frequency filter for third mode extraction. (b) Spectrogram of extracted third modal arrival. (c) Residual signal after first iteration. (d) Time-frequency filter for second mode extraction. (e) Spectrogram of extracted second modal arrival. (f) Residual signal after second iteration. (g) Time-frequency filter for fourth mode extraction. (h) Spectrogram of extracted fourth modal arrival. (i) Residual signal $=$ 1st modal arrival.

lights less energetic components. It is a consequence of filtering out the first two most energetic components. This property of the proposed methodology proves its usefulness for signals composed of several arrivals with large differences of magnitude. This issue will be illustrated in Section V in the case of real data.

V. Results

In this section, we illustrate how the methodology proposed in this paper performs in the case of real signals. The dataset contains North Atlantic right whale vocalizations recorded in the Bay of Fundy during 2000 and 2002 [23]. Recordings were performed by four autonomous hydrophones moored on the bottom and disposed as indicated in Fig. 13. The purpose of the experiment was to estimate the transmitter position by analyzing signals received by the hydrophones. The transmitted signal is similar to a transient generated by an explosion. Due to the dispersion of the channel, the signals arrived at each hydrophone are composed of several modal arrivals as shown in Fig. 14.

The approximative position of the source has been established from visual observations. However, as it is shown in this section,

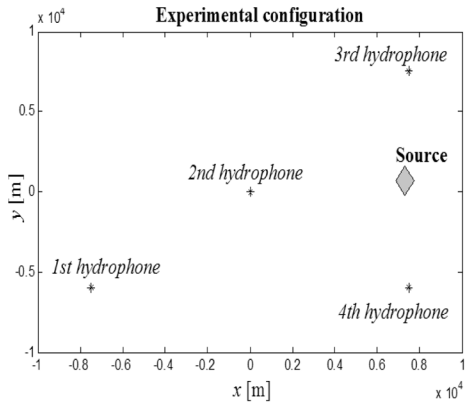

Fig. 13. Experimental configuration: hydrophones positions with respect to the source ($\mathrm{Depth} \approx 130\,\mathrm{m}$).

several locating methods have been used in order to get this position which is actually the final goal of this application.

While the signal transmitted by sources (right whales) is at very low frequencies (transient below 100 Hz) the source local-

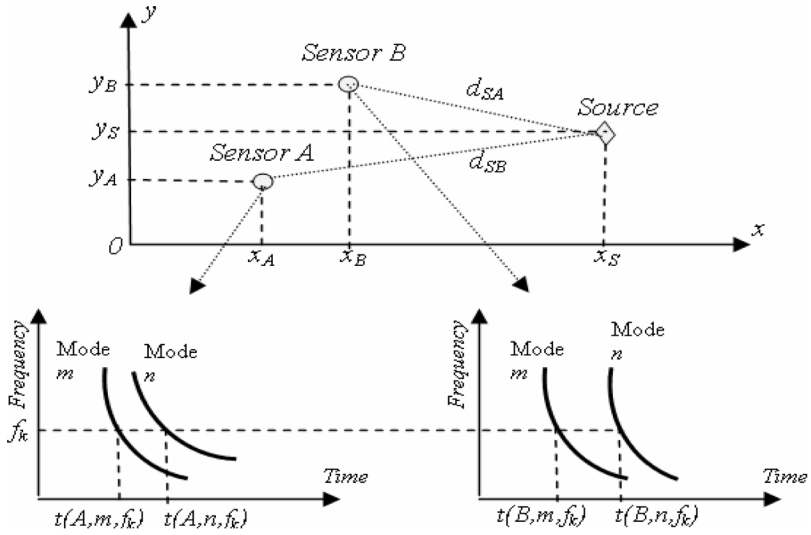

Fig. 14. Localization principle based on modes time-of-arrivals (TOA) estimation.

ization algorithm requires the extraction of modal arrivals from the signals received by each of the sensors. The blind localization method, introduced in [23], is based on the estimation of relative delays between modal arrivals received by sensor network. Let us consider two modes at two sensors—Fig. 14.

The relative time of arrival TOAs between two modes received by the sensors are proportional to the distance between source and each of these sensors. According to [23] the TOAs of signals received by the sensors A and B are expressed as

$$\begin{aligned} t(A,m,f) &= t_S(f) + \frac{d_{\mathrm{SA}}}{v_g(m,f)} \\ t(B,m,f) &= t_S(f) + \frac{d_{\mathrm{SB}}}{v_g(m,f)} \end{aligned} \tag{19}$$

where $t_{\mathrm{S}}(f)$ is the group delay of the transmitted signal. The relative time of arrival between two modes is independent of the $t_{\mathrm{S}}(f)$ as shown by

$$\begin{aligned} &\text{Sensor A}: dt(A,m,n,f) = t(A,n,f) - t(A,m,f) \\ &\quad = d_{\mathrm{SA}}\left(\frac{1}{v_g(n,f)} - \frac{1}{v_g(m,f)}\right) \\ &\text{Sensor B}: dt(B,m,n,f) = t(B,n,f) - t(B,m,f) \\ &\quad = d_{\mathrm{SB}}\left(\frac{1}{v_g(n,f)} - \frac{1}{v_g(m,f)}\right). \end{aligned} \tag{20}$$

Furthermore, the ratio between the relative TOAs of the same mode, computed for two sensors, is completely independent of the propagation parameters (materialized by the group velocity v_g):

$$\begin{aligned} R(A,B,m,n,f) &= \frac{t(A,n,f) - t(A,m,f)}{t(B,n,f) - t(B,m,f)} = \frac{d_{\mathrm{SA}}}{d_{\mathrm{SB}}} \\ &= \frac{\sqrt{(x_s - x_A)^2 + (y_s - y_A)^2}}{\sqrt{(x_s - x_B)^2 + (y_s - y_B)^2}}. \end{aligned} \tag{21}$$

The estimation of the time-frequency structures of the modal arrivals provides an estimation of this ratio, based on the times of arrival obtained for each frequency f_k:

$$R(A,B,m,n,f_k) = \frac{t(A,n,f_k) - t(A,m,f_k)}{t(B,n,f_k) - t(B,m,f_k)}. \tag{22}$$

The source localization can then be posed as the optimization problem described by [14]

$$(x_s, y_s) = \underset{(m,n),(i,j),f_k}{\arg\min}\, J(x,y,(m,n),(i,j),f_k) \tag{23}$$

where J is the multidimensional objective function defined as

$$\begin{aligned} J(x,y,(m,n),(i,j),f_k) &= (x_s - x_i)^2 + (y_s - y_i)^2 \\ &\quad - R^2(A,B,m,n,f_k)\left[(x_s - x_j)^2 + (y_s - y_j)^2\right] \end{aligned} \tag{24}$$

where $\{(m,n)\}$ is the set of mode pairs, $\{(i,j)\}$ is the set of sensors pairs. The estimations obtained between several modes and several sensors pairs reduce the error in the estimation due to the noise, arbitrary attenuations of modes, source position ambiguities, etc. (see [23] for more details).

One recording of a whale vocalization received by the sensor network illustrated in Fig. 13 is considered in the following example. The spectrograms of signals received by the four sensors are plotted in Fig. 15.

This figure illustrates a good fitting between the estimated modes, provided by the methodology proposed in this paper and the spectrograms. The time-frequency-phase continuity criteria show their ability to correctly estimate the time-frequency structures located very close each other.

Fig. 16 illustrates the comparisons between the estimated modes received by the sensor 1 and 4 and the modes obtained by simulations using Kraken program in the bandwidth 27–65 Hz (according to the physical configuration defined in this section).

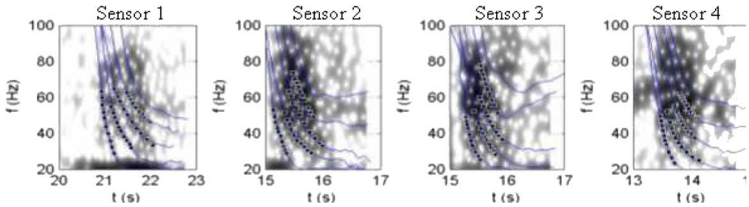

Fig. 15. Mode estimations (blue line) from signal received by sensors.

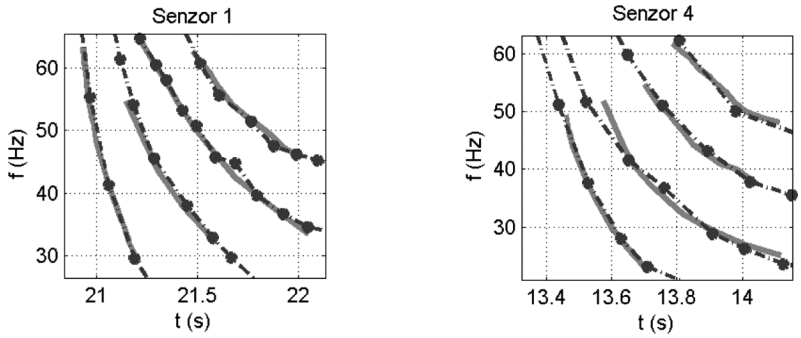

Fig. 16. Comparison of the extracted modal arrivals (dashed line) with the modes obtained from physical modelling (solid lines).

TABLE I
COMPARATIVE LOCALIZATION RESULTS

Method	x [m]	y [m]
Desharnais et al. [24] ×	8884	-848
Laurinelli et al. [25] ●	8950	-970
Proposed method +	8300	-986

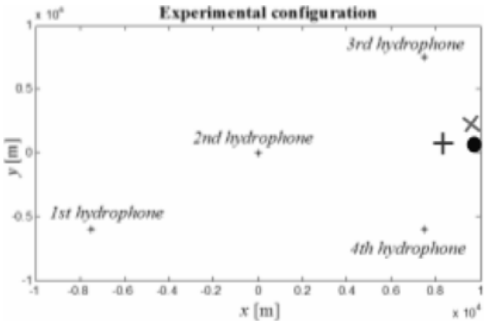

Fig. 17. Comparison of localization results of the three methods.

We can remark that the estimated modal arrivals are close to the simulated ones proving also that the results provided by the proposed method correspond to physical modes. The relative small errors could be explained by the differences between simulation and the model assumed by our approach and real conditions.

In order to prove the accuracy of our methodology, the estimations of time-frequency structures of received signals (Fig. 15) have been used for the localization, based on the algorithm described above. While the dataset corresponds to real whale vocalizations the real position of the source is unknown. For this reason, we compare the localization results provided by the proposed method with the ones obtained by other methods [24], [25]. This comparison is illustrated in Fig. 16 and the Table I gives the estimated positions by the three methods considered.

As illustrated by Fig. 17, the three methods localize the source in the same region of the considered area. Of course, there are differences between these results (Table I), but the three estimations are close with respect of the investigated area. However, without knowledge of the actual source position, it is difficult to state which the method is most accurate. In this context, the main advantage of the method proposed by this paper is the performance without any knowledge about acoustic properties of the channel. That is, we did not assume any propagation models as often used by model matching-based techniques. The time-frequency structures are extracted only taking advantage of their coherence materialized by the continuity in time-frequency domain. Nevertheless, this localization method assumes that the physical properties (bathymetry, sound speed in sediment and water column) are the same between the sources and hydrophones. The eventual variations of these parameters as well the range variability will be considered in the further work.

VI. CONCLUSION AND PERSPECTIVES

In this paper, a methodology of time-frequency component extraction has been proposed. Its main feature is the enhanced performance for complex signals with weak assumptions about their contents. Hence, using some time-frequency-phase local continuity criteria, universal for a broad class of signals, allows the estimation of the time-frequency structures of signal's components. Furthermore, these shapes are used to calibrate a time-varying filter which iteratively extracts each component. The proposed method could be seen as a new version of matching pursuit algorithm where the best matched structure is found by considering the component characterized by arbitrary but *continuous* time-frequency shapes. More precisely, it is known that the matching pursuit algorithm performs, at each iteration, the subtraction of the best fitted component from the signal. Such an operation requires the estimation of the magnitude of the

best fitted component, which is generally a complex task. Alternatively, the nonstationary filtering procedure provided by the proposed method, avoids the need for component amplitude estimation. The extraction of signal's component is provided by filtering instead of subtraction.

This method has been applied to the dispersive underwater environment. Since no physical assumption is required by the proposed method, it could be generalized for any other dispersive system. The analyzed signal is composed of several modes having different nonlinear time-frequency structures, usually located below the resolution capability of existing methods. In this context, looking for local time-frequency-phase continuity allows connecting time-frequency local atoms in order to identify the time-frequency shape of a given component. The energies of modes being very different, the physical separation of component is done by filtering each of them according to the time-frequency shape previously estimated.

While characterized by high resolution capabilities (with respect of spectrogram or wavelet based methods), the proposed method could be interesting in short range transmitter–receiver configurations which are characterized by very close time-frequency structures. This could be combined with the methodology proposed in [26] allowing the tomographic inversion of sediments in shallow water even for short ranges.

The results provided for synthetic and real data prove the capability of the proposed methodology to efficiently perform in the context of multicomponent signals having nonlinear time-frequency structures. We have also shown its application to the right whale localization.

In the future, we will focus on developing new techniques for taking advantage on time-frequency-phase continuity. The uses of a local polynomial phase modeling or new filtering technique are two areas of further work in this field. We also intend to apply this technique for other real datasets. New applications based on dispersive modal diversity will be also investigated for blind localization or efficient communication scheme in low frequency underwater environment.

ACKNOWLEDGMENT

The authors would like to thank the organizers of the First Workshop on Classification and Localisation of Underwater Mammals, Dartmouth, NS, Canada, November 19–21, 2003, and Prof. Simard of the Institute des Science de la Mer, Rimouski, Canada, for the real datasets used in their works.

REFERENCES

[1] I. Tolstoy and C. S. Clay, *Ocean Acoustics: Theory and Experiments in Underwater Sound*. New York: McGraw-Hill, 1966.

[2] B. G. Iem, A. Papandreou-Suppappola, and G. F. Boudreaux-Bartels, "Wideband weyl symbols for dispersive time-varying processing of systems and random signals," *IEEE Trans. Signal Process.*, vol. 50, no. 5, pp. 1077–1090, May 2002.

[3] A. M. Sayeed and B. Aazhang, "Communications over multipath fading channels: A time-frequency perspective," in *Wireless Communications: TDMA versus CDMA*. Norwell, MA: Kluwer, 1997, pp. 73–98.

[4] Y. Jiang and A. Papandreou-Suppappola, "Discrete time-frequency characterizations of dispersive time-varying systems," *IEEE Trans. Signal Process.*, vol. 55, no. 5, pp. 2066–2076, May 2007.

[5] Y. Jiang and A. Papandreou-Suppappola, "Discrete time-scale characterization of wideband time-varying systems," *IEEE Trans. Signal Process.*, vol. 54, no. 4, pp. 1364–1375, Apr. 2006.

[6] G. V. Frisk, *Ocean and Seabed Acoustics*. Englewood Cliffs, NJ: Prentice-Hall, 1994.

[7] A. Jarrot, C. Ioana, and A. Quinquis, "Toward the use of the time-warping principle with discrete-time sequences," *J. Comput.*, vol. 2, *6*, pp. 49–55, 2007.

[8] M. Stojanovic, *Acoustic Underwater Communications, Entry in Encycolpedia of Telecommunications*, J. G. Proakis, Ed. New York: Wiley, 2003.

[9] E. K. Westwood, C. T. Tindle, and N. R. Chapman, "A normal mode model for acousto-elastic ocean environments," *J. Acoust. Soc. Amer.*, vol. 100, pp. 3531–3645, 1996.

[10] I. Csiszár and F. Matus, "Information projections revisited," *IEEE Trans. Inf. Theory*, vol. 49, no. 6, pp. 1474–1490, Jun. 2003.

[11] J. C. Lagarias, J. A. Reeds, M. H. Wright, and P. E. Wright, "Convergence properties of the Nelder-Mead simplex method in low dimensions," *SIAM J. Optim.*, vol. 9, no. 1, pp. 112–147, 1998.

[12] A. Jarrot, C. Ioana, and A. Quinquis, "A time-frequency characterization framework for signals issued from underwater dispersive environments," presented at the IEEE Int. Conf. Acoustics, Speech, Signal Processing, Honolulu, HI, Apr. 2007.

[13] B. Boashash and P. O'Shea, "Polynomial Wigner–Ville distributions and their relationship to time-varying higher order spectra," *IEEE Trans. Signal Process.*, vol. 42, no. 1, pp. 216–220, Jan. 1994.

[14] LJ. Stankovic, "On the realization of the polynomial Wigner–Ville distribution for multicomponent signals," *IEEE Signal Process. Lett.*, vol. 5, pp. 157–159, Jul. 1998.

[15] B. Barkat and B. Boashash, "Instantaneous frequency estimation of polynomial FM using the peak of the PWVD: Statistical performance in the presence of additive Gaussian noise," *IEEE Trans. Signal Process.*, vol. 47, no. 9, pp. 2480–2490, Spe. 1999.

[16] S. Peleg and B. Porat, "Estimation and classification of polynomial phase signal," *IEEE Trans. Inf. Theory*, vol. 37, pp. 422–430, Mar. 1991.

[17] S. Barbarossa, A. Scaglione, and G. B. Giannakis, "Product high-order ambiguity function for multicomponent polynomial-phase signal modeling," *IEEE Trans. Signal Process.*, vol. 46, no. 3, pp. 691–708, Mar. 1998.

[18] A. Papandreou, S. M. Kay, and G. F. Boudreaux-Bartels, "The use of hyperbolic time-frequency representation for optimum detection and parameter estimation of hyperbolic chirps," in *Proc. IEEE-SP Symp. Time-Frequency/Time-Scale*, Philadelphia, PA, Oct. 1994, pp. 512–518.

[19] F. Hlawatsch, A. Papandreou, and G. F. Boudreaux-Bartels, "The power classes-quadratic time-frequency representations," *IEEE Trans. Signal Process.*, vol. 47, no. 11, pp. 3067–3083, Nov. 1999.

[20] F. Hlawatsch, G. Matz, H. Kirchauer, and W. Kozej, "Time-frequency formulation, design, and implementation of time-varying optimal filters for signal estimation," *IEEE Trans. Signal Process.*, vol. 48, no. 5, pp. 1417–1432, May 2000.

[21] S. Peleg and B. Friedlande, "Multicomponent signal analysis suing the polynomial-phase transform," *IEEE Trans. Signal Process.*, vol. 43, no. 8, pp. 1901–1914, Aug. 1995.

[22] F. Cakrak and P. J. Loughlin, "Multiple window time-varying spectral analysis," *IEEE Trans. Signal Process.*, vol. 49, no. 2, pp. 448–453, Feb. 2001.

[23] C. Gervaise, S. Vallez, Y. Stephan, and Y. Simard, "Robust 2-D localization of low-frequency calls in shallow waters using modal propagation modelling," *Canad. Acoust. J.*, Nov. 2007, accepted for publication.

[24] F. Desharnais, M. Côté, C. J. Calnan, G. R. Ebbeson, D. J. Thomson, N. E. B. Collison, and C. A. Gillard, "Right whale localisation using a downhill simplex inversion scheme," *Canad. Acoust.*, vol. 32, no. 2, pp. 137–145, 2004.

[25] M. H. Laurinelli and A. Hay, "Localisation of right whale sounds in the workshop Bay of Fundy dataset by spectrogram cross-correlation and hyperbolic fixing," *Canad. Acoust.*, vol. 32, no. 2, pp. 132–136, 2004.

[26] M. I. Taroudakis and M. G. Markaki, "On the use of matched-field processing and hybrid algorithms for vertical slice tomography," *J. Acoust. Soc. Amer.*, vol. 102, pp. 885–895, 1997.

[27] G. R. Potty, J. H. Miller, J. Lynch, and K. Smith, "Tomographic inversion for sediment parameters in shallow water," *J. Acoust. Soc. Amer.*, vol. 108, pp. 973–986, 2000.

Cornel Ioana received the Dipl.-Eng. degree in electrical engineering from the Romanian Military Technical Academy of Bucharest, Romania, in 1999 and the M.S. degree in telecommunication science and the Ph.D. degree in the electrical engineering field, both from University of Brest-France, in 2001 and 2003, respectively.

Between 1999 and 2001, he activated as a Military Researcher in a research institute of the Romanian Ministry of Defense (METRA), Bucharest, Romania. Between 2003 and 2006, he worked as Researcher and Development Engineer in ENSIETA, Brest, France. Since 2006, he has been an Associate Professor-Researcher with the Grenoble Institute of Technology/GIPSA-lab. His current research activity deals with the signal processing methods adapted to the natural phenomena. His scientific interests are nonstationary signal processing, natural process characterization, underwater systems, electronic warfare, and real-time systems.

Arnaud Jarrot received the Dipl.–Eng degree in electrical engineering from the Institut National des Sciences Appliquées (INSA), Lyon, France, in 2003. He is currently working towards the Ph.D. degree at the Ecole Nationale Supérieure des Ingénieurs des Etudes des Techniques d'Armement (ENSIETA), Brest, France. His area of interest are signal processing, time-frequency methods and nonstationary and nonlinear filtering with a focus on real-world applications.

Cédric Gervaise received the Ph.D. degree in signal processing from the Université Paul Sabatier, Toulouse, France, in 1999, the M.Sc. degree in electrical engineering from the Université Paul Sabatier, Toulouse, France, in 1996, and the Engineer degree in aeronautics from ENSICA Toulouse, France, in 1994.

He is currently a Researcher in ENSIETA, where he is head of the passive underwater acoustics team of New Technologies development. He was a visiting Scholar at the Fisheries&Oceans, Canada, bioacoustics team in 2009. His research topics are underwater acoustics, signal processing for passive acoustical oceanography, and the design of underwater observatories. He is author and coauthor of 15 publications in refereed journals (published or in press) and is the supervisor of three Ph.D. candidates

Yann Stéphan was born in Lannion, France, in 1966. He received the Engineering diploma in electrical engineering from Ecole Nationale Supérieure des Ingénieurs Electriciens de Grenoble (ENSIEG), Grenoble, France, in 1991 and the Ph.D. degree in computer sciences from Conservatoire National des Arts et Metiers (CNAM), Paris, France, in 1996.

Since 1992, he has worked with the Service Hydrographique et Océanographique de la Marine (SHOM) within the Military Oceanography Department, Brest, France. His current interests include inverse methods, acoustic environmental assessment, and tactical use of the environment.

André Quinquis received the M.S. degree and the Ph.D. degree in signal processing, both from the University of Brest, Brest, France, in 1986 and 1989, respectively.

From 1992 to 2007, he taught and developed research activities in signal processing at the Engineering School Ecole Nationale Supérieure d'Ingénieurs des Etudes et techniques d'Armement (ENSIETA) of Brest, Brest, France. He held the positions of Senior Researcher and head of the research laboratory Extraction et Exploitation d l'Information en Environnements Incertains. From 2001 to 2007, he held the position of Scientific Director of ENSIETA. Since 2007, he joined the French armament procurement agency (DGA). He held the position of manager in charge of valuation of the basic R&T project grants. He is author of 11 books and more than 130 papers (international journals and conferences) in the area of signal processing. He is mainly interested in passive systems such as radar and sonar processes.